Stability and electronic structure studies of $LaAlO_3/SrTiO_3$ (110) heterostructures*

Du Yan-Ling(杜颜伶)[a)b)], Wang Chun-Lei(王春雷)[a)], Li Ji-Chao(李吉超)[a)†], Xu Pan-Pan(徐攀攀)[a)], Zhang Xin-Hua(张新华)[a)], Liu Jian(刘 剑)[a)], Su Wen-Bin(苏文斌)[a)], and Mei Liang-Mo(梅良模)[a)]

[a)] *School of Physics, State Key Laboratory of Crystal Materials, Shandong University, Jinan* 250100, *China*
[b)] *College of Science and Technology, Shandong University of Traditional Chinese Medicine, Jinan* 250355, *China*

(Received 8 November 2013; revised manuscript received 17 February 2014; published online 10 June 2014)

The first-principles calculations are employed to investigate the stability, magnetic, and electrical properties of the oxide heterostructure of $LaAlO_3/SrTiO_3$ (110). By comparing their interface energies, it is obtained that the buckled interface is more stable than the abrupt interface. This result is consistent with experimental observation. At the interface of $LaAlO_3/SrTiO_3$ (110) heterostructure, the Ti–O octahedron distortions cause the Ti t_{2g} orbitals to split into the two-fold degenerate d_{xz}/d_{yz} and nondegenerate d_{xy} orbitals. The former has higher energy than the latter. The partly filled two-fold degenerate t_{2g} orbitals are the origin of two-dimensional electron gas, which is confined at the interface. Lattice mismatch between $LaAlO_3$ and $SrTiO_3$ leads to ferroelectric-like lattice distortions at the interface, and this is the origin of spin-splitting of Ti 3d electrons. Hence the magnetism appears at the interface of $LaAlO_3/SrTiO_3$ (110).

Keywords: two-dimensional electron gas, $LaAlO_3/SrTiO_3$ (110) interface, magnetic interface

PACS: 73.20.–r, 75.70.Cn, 68.35.Md **DOI:** 10.1088/1674-1056/23/8/087302

1. Introduction

In recent years, a transition-metal oxide heterostructure $LaAlO_3/SrTiO_3$ has attracted lots of attention due to its novel electronic properties at the interface such as metallicity,[1] superconductivity,[2] and magnetism.[3] Furthermore, its metallic phase has a very high carrier density and mobility,[1,4] and therefore can be regarded as two-dimensional electron gas (2DEG). For this 2DEG, its magnetic phase was first suggested by Brinkman *et al.*,[3] who deduced the presence of magnetism from the temperature dependence of the interface resistance R, and a hysteresis of R during the sweep of a magnetic field H. Recently, magnetic phase was found above room temperature.[5] Moreover, direct evidence for in-plane ferromagnetic order at the interface was found by Lee *et al.*[6] In earlier reports, the magnetic and superconducting phases were observed separately in different samples.[2,3] However, other groups have provided the direct evidence of the coexistence of the two phases in the same sample recently.[7–11] Meanwhile the mechanism of coexistence of magnetism and superconductivity is still unclear. So far, most of researches are focused on properties of $LaAlO_3/SrTiO_3$ (001) heterostructures, and the properties of $LaAlO_3/SrTiO_3$ (110) interface lack investigation.

The conductivity at $LaAlO_3/SrTiO_3$ (001) interface has been explained by the electronic reconstruction. It is a direct consequence of the polar discontinuity resulting from the sudden transition from nonpolar ($SrTiO_3$) to polar ($LaAlO_3$) material.[12–14] On the other hand, for the case of $LaAlO_3/SrTiO_3$ (110) heterostructures, both the $SrTiO_3$ and $LaAlO_3$ can be represented by planar stacks of $[ABO]^{4+}$ and $[O_2]^{4-}$ layers,[15] and there are no polarization discontinuities at the interfaces.[16] Based on the polar catastrophe theory, there should be neither electronic reconstruction nor two-dimensional electron gas (2DEG) formed at $LaAlO_3/SrTiO_3$ (110) interface. However, the 2DEG has been observed indeed at $LaAlO_3/SrTiO_3$ (110) interfaces in recent experiments.[16,17] The mechanism of 2DEG formed at the interface is still debated, and the study of the origin of 2DEG is conducible to understanding the physics connotation of these interfaces. In addition, as is well known, the interface properties are determined by the interface structure. In the process of heteroepitaxial growth, many factors, such as the lattice constants, surface energies, and interface energies of the epitaxy materials and substrates can lead to different growth patterns in the epitaxial layer, and influence the interface properties. In this work, possible geometric structure at the $LaAlO_3/SrTiO_3$ (110) interface is investigated by comparing interface energies of different structures. Then, electrical and magnetic properties of the $LaAlO_3/SrTiO_3$ (110) interface are studied by analyzing its electronic structures.

2. Model and method

$SrTiO_3$ (110) surface is modeled as seven alternating SrTiO and O–O (denoted as O_2 hereafter) layers as shown in

*Project supported by the National Basis Research Program of China (Grant No. 2013CB632506), the National Natural Science Foundation of China (Grant Nos. 11374186, 51231007, and 51202132), and the Independent Innovation Foundation of Shandong University, China (Grant No. 2012TS027).

†Corresponding author. E-mail: lijichao@sdu.edu.cn

© 2014 Chinese Physical Society and IOP Publishing Ltd

Fig. 1. This model is symmetric about the middle of the slabs with two types of terminations. One is terminated by O_2 layer as shown in Fig. 1(a), and the other is terminated by SrTiO layer as shown in Fig. 1(b). These slabs are nonstoichiometric, with unit cell formulas as $Sr_5Ti_5O_{17}$ terminated by O_2 layer and $Sr_5Ti_5O_{13}$ terminated by SrTiO layer. A similar model is constructed for $LaAlO_3$ (110) surfaces as shown in Figs. 1(c) and 1(d). These slabs are designed as symmetric structures because they would lead to a large dipole moment if the slabs are asymmetric with different terminations, such as SrTiO–O_2–SrTiO–O_2–SrTiO–O_2. It is much more likely that the surfaces of asymmetric slabs might become metallic in order to avoid the infinite electrostatic energy arising from such surface charges, and then, the surface energy would be quite high.[18–21]

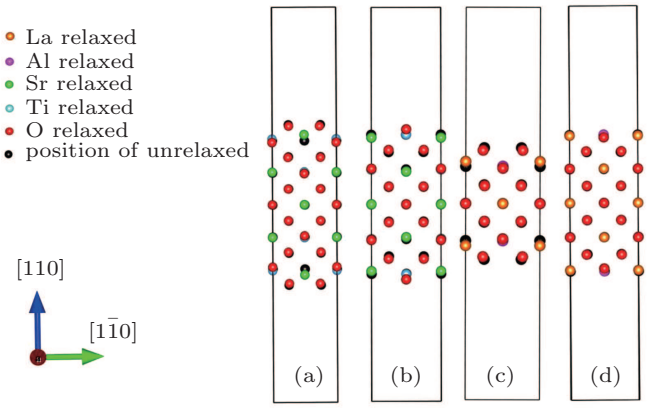


Fig. 1. (color online) Relaxed and unrelaxed $SrTiO_3$ and $LaAlO_3$ slabs from our calculations. (a) $SrTiO_3$ slab terminated by O_2 layer; (b) $SrTiO_3$ slab terminated by SrTiO layer; (c) $LaAlO_3$ slab terminated by O_2 layer; (d) $LaAlO_3$ slab terminated by LaAlO layer.

Symmetric slabs are formed for $LaAlO_3/SrTiO_3$ (110) interfaces. For abrupt interface structure (SrTiO–O_2–LaAlO), there are two possible terminated layers: the LaAlO-terminated and the O_2-terminated as shown in Figs. 2(a) and 2(b). In recent experiments,[16] a buckled interface structure (SrTiO–O_2–LaTiO–O_2–LaAlO) has been proposed. The buckled interface structure also has two possible terminated layers: the LaAlO-terminated and the O_2-terminated, which are shown in Figs. 2(c) and 2(d) respectively. These models are nonstoichiometric. For the abrupt interface structures, the unit cell formulas are $Sr_3La_6Ti_3Al_6O_{25}$ terminated by LaAlO layer and $Sr_3La_6Ti_3Al_6O_{29}$ terminated by O_2 layer. For the buckled interface structures, the unit cell formulas are $Sr_3La_6Ti_5Al_4O_{25}$ terminated by LaAlO layer and $Sr_3La_6Ti_5Al_4O_{29}$ terminated by O_2 layer. A vacuum spacing of 20 Å between adjacent slabs is included in each of heterostructures to avoid interaction between two slabs.

In this work, all calculations are carried out using the projector augmented wave (PAW) approach.[22] A plane wave basis is implemented in the Vienna *ab initio* Simulation Package (VASP).[23,24] The calculations of stability are carried out using density functional theory within the local density approximation (LDA). During the calculation of electronic structure, the exchange correlation effects are treated within the rotational invariant LDA + U approach of Liechtenstein *et al.*,[25] which includes a Hubbard U term accounting for the on-site Coulomb interaction, with $U = 5.00$ and $J = 0.64$ eV for the Ti d states,[26] and with $U_f = 11.00$ eV and $J_f = 0.68$ eV for the La f states.[10] For Sr and Ti, we use PAW potentials in which semicore states are treated as valence states ($Sr_{_sv}$ and $Ti_{_pv}$ in the VASP distribution). For La and O, we use standard potentials (La and O in the VASP distribution). Bulk and heterostructure calculations are performed using the 5×5×5 and 5×4×1 Monkhorst–Pack[27] k-point mesh, respectively. Plane waves include up to an energy cut off of 500 eV, and all the atomic positions are fully relaxed until atomic forces are less than 0.01 eV/Å.

3. Results and discussion

3.1. Interface stability

For surface energy calculations, $SrTiO_3$ (110) surfaces are chosen as an example to demonstrate our calculations. The cleavage energy $E_{cl}(\zeta)$ (ζ denotes the structure terminated by a layer: SrTiO or O_2) can be obtained through the following equation:

$$E_{cl}(\zeta) = \frac{1}{4}\left[E_{slab}(O_2) + E_{slab}(SrTiO) - N \cdot E_{buck}\right], \quad (1)$$

where factor 1/4 means that there are totally four surfaces, $E_{slab}(O_2)$ is the total energy of the unrelaxed slabs terminated by O_2 layer, $E_{slab}(SrTiO)$ is the total energy of the unrelaxed slabs terminated by SrTiO layer, and E_{bulk} is the energy per formula unit in the cubic structure.

The relaxation energy $E_{rel}(\zeta)$ of each surface can be obtained from the following equation:

$$E_{rel}(\zeta) = \frac{1}{2}\left[E^{rel}_{slab}(\zeta) - E^{unrel}_{slab}(\zeta)\right], \quad (2)$$

where factor 1/2 means that there exist totally two surfaces, $E^{rel}_{slab}(\zeta)$ is the total energy of the relaxed slabs terminated by ζ layer, and $E^{unrel}_{slab}(\zeta)$ is the total energy of the unrelaxed slabs.

The surface energy is a sum of the cleavage energy and the relaxation energy, i.e.,[21]

$$E_{surf}(\zeta) = E_{cl}(\zeta) + E_{rel}(\zeta). \quad (3)$$

The interface energy $E_{inter}(\delta)$ (δ is the heterostructure with abrupt interface or buckled interface, as shown in Fig. 2) can be obtained from the following equation:

$$E_{inter}(\delta) = \frac{1}{4}[E(LaAlO) + E(O_2) - 2E_{surf}(LaAlO) - 2E_{surf}(O_2) - E_{bulk}], \quad (4)$$

where factor 1/4 means that there exist totally four interfaces. $E(LaAlO)$ and $E(O_2)$ are the total energies of the relaxed

slabs, which are terminated by LaAlO layer and O_2 layer, respectively, E_{surf}(LaAlO) and E_{surf} (O_2) are the surface energies of the slabs, which are terminated by LaAlO layer and O_2 layer, respectively, the factor 2 before E_{surf} means that there exist two surfaces. E_{bulk} is the sum of the bulk energy per formula unit in the cubic structure.

As shown in Fig. 1, for $SrTiO_3$ (110) surface with O_2-terminated layer, the upper layer oxygen ions relax inwards, and the second layer is folded significantly as the strontium and titanium ions relax outwards while the oxygen ion relaxes inwards. For $SrTiO_3$ (110) surface with SrTiO-terminated layer, the upper layer is folded significantly as the strontium ion relaxes inward while the oxygen ion relaxes outward. For all $SrTiO_3$ (110) surfaces, the displacements of atoms rapidly decrease as atoms enter into the bulk. Our results are consistent with previous calculations.[18] For $LaAlO_3$ (110) surface, many relaxations similar to those for $SrTiO_3$ (110) surface have been obtained, including that in the upper layer oxygen ions relax inwards strongly and in the second layer that is folded significantly, the lanthanum and aluminum ions relax outwards while the oxygen ion relaxes inwards when the surface is terminated by O_2 layer. But for $LaAlO_3$ (110) surface with LaAlO-terminated layer, in the upper layer that is folded significantly, lanthanum ion relaxes outwards while oxygen ion relaxes inwards, which is different from the scenario for $SrTiO_3$ (110) surface with SrTiO-terminated layer. Along the (110)-orientation, there is a large magnitude of the polar discontinuity at each of these surfaces. And the polar discontinuity surface causes all these atoms to displace, since it can strongly enhance the driving force for the formation of charge-neutral surfaces.[28] The calculated cleavage energies, relaxation energies, and surface energies for different terminations of $SrTiO_3$ (110) and $LaAlO_3$ (110) surfaces are listed in Table 1. From Table 1, it can be seen that the O_2-terminated surface is more stable no matter whether the surface energies of O_2-terminated surface for $SrTiO_3$ (110) surface or $LaAlO_3$ (110) surface are much lower than those for $SrTiO_3$ (110) surface and $LaAlO_3$ (110) surface.

Table 1. Calculated cleavage energies, relaxation energies, and surface energies in J/m^2 for different terminations of $SrTiO_3$ (110) and $LaAlO_3$ (110) surfaces.

Surface	Terminating layer	$E_{(cl)}$	$E_{(rel)}$	$E_{(surf)}$
$SrTiO_3$ (110)	SrTiO	5.059	–0.607	4.452
	O_2	5.059	–0.691	4.368
$LaAlO_3$ (110)	LaAlO	5.223	–0.097	5.126
	O_2	5.223	–0.687	4.536

Figure 2 shows that the calculated results of structural relaxation of $LaAlO_3$/$SrTiO_3$ (110) heterostructure. Figures 2(a) and 2(b) show the abrupt interface structures (SrTiO–O_2–LaAlO) with two possible terminated layers: the LaAlO-terminated layer and the O_2-terminated layer, respectively. Figures 2(c) and 2(d) show the buckled interface structures (SrTiO–O_2-LaTiO–O_2-LaAlO) with two possible terminated layers: the LaAlO-terminated layer and the O_2-terminated layer, respectively. It can be easily seen that the structural relaxation occurs primarily in the $LaAlO_3$ slab. The structural relaxation at the surface of $LaAlO_3$ is much obvious than that at the interface of $LaAlO_3$/$SrTiO_3$. In addition, we can see that the surface atomic displacements of the heterostructures with abrupt interfaces are more significant than those of the heterostructures with buckled interfaces. The two interface energies are calculated and listed in Table 2. From Table 2, it can be seen that $LaAlO_3$/$SrTiO_3$ (110) heterostructure with buckled interfaces is more stable than that of the abrupt interfaces, since the interface energy of the buckled interface is much lower than that of the abrupt interface. Our calculations offer a direct theoretical confirmation for the previous experiment observations.[16]

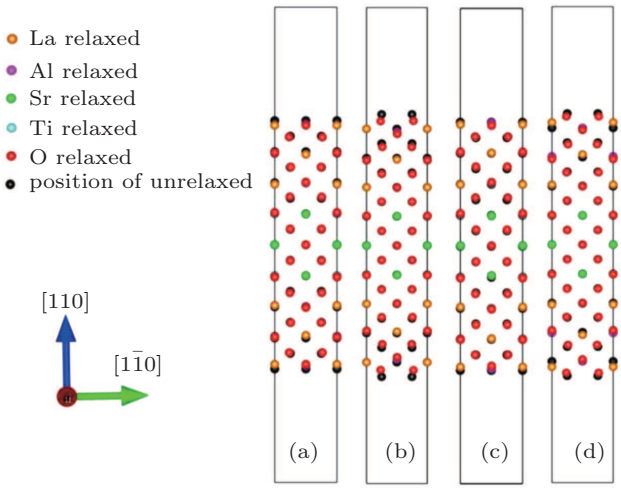


Fig. 2. (color online) Relaxed and unrelaxed $SrTiO_3$/$LaAlO_3$ interfaces from our calculations. (a) The abrupt interface structure (SrTiO–O_2–LaAlO) terminated by LaAlO; (b) The abrupt interface structure (SrTiO–O_2–LaAlO) terminated by O_2; (c) The buckled interface structure (SrTiO–$O_2$0-LaTiO–O_2–LaAlO) terminated by LaAlO; (d) the buckled interface structure (SrTiO–O_2-LaTiO–O_2–LaAlO) terminated by O_2.

Table 2. Calculated interface energies in J/m^2 for $LaAlO_3$/$SrTiO_3$ (110) interfaces.

Interface	Interface energy/(J/m$^{2)}$
Abrupt interface	0.170
Buckled interface	–0.952

3.2. Electronic structures

Model shown in Fig. 3 is constructed to investigate the magnetic and electrical properties of the buckled $LaAlO_3$/$SrTiO_3$ (110) interface. To minimize the interaction between the interfaces, we use thicker slabs containing five $LaAlO_3$ and $SrTiO_3$ layers between adjacent interfaces. Figure 3 also shows the atomic positions of the relaxed structure and the unrelaxed structure. For the anion and the cation,

the displacements from the ideal structure are not equal, indicating that there is a ferroelectric-like distortion of the Ti–O octahedron, especially at the interface. The largest displacement, which is about 0.26 Å, occurs at O anion of the interface layer, while the displacement of Ti atom in the interface layer is about 0.15 Å.

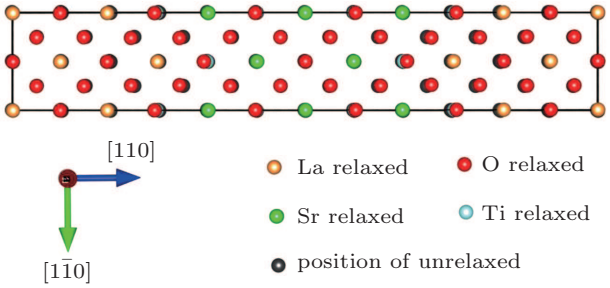


Fig. 3. (color online) Relaxed and unrelaxed structures of $LaAlO_3/SrTiO_3$ (110) interface.

The total density of states (TDOS) is shown in Fig. 4(a), and the partial density of states (PDOS) of the Ti 3d states at the interface is shown in Fig. 4(b). From Fig. 4(a), it can be seen that n-type metallic state is obtained since there are occupied conducting states near the Fermi energy. On the other hand, the unbalance of the spin-up and spin-down states occurs and yields magnetic property. From Fig. 4(b), it can be seen that the two-fold degenerate d_{xz}/d_{yz} of the interface Ti 3d orbitals dips below the Fermi level, thereby forming a 2DEG. The unbalance of the spin-up and spin-down states yields a magnetic moment of about 0.35 μB on the Ti atom of the interface. Thus the Ti 3d states at the interface contribute greatly to the metallic and magnetic properties of $LaAlO_3/SrTiO_3$ (110) heterostructure.

Figure 5(a) shows the relaxed $LaAlO_3/SrTiO_3$ (110) heterostructure with buckled interfaces the same as those in Fig. 3. The PDOS layers are shown in Fig. 5(b), and the labels for each layer of the PDOS are aligned like those in Fig. 5(a). From Fig. 5(b), it can be seen that a 2DEG emerges at the interface, since the largest occupied PDOS near the Fermi energy occurs at the interface and the occupation number decreases when moving away from the interface. Furthermore, the unbalance of the spin-up and spin-down states occurs primarily at the interface. Our results are in agreement with previous experimental results.[16,17] However, there are two main differences between Fig. 5(b) in our work and Fig. 5(c) in Ref. [16]. First, our work considers the magnetic and electrical properties of the $LaAlO_3/SrTiO_3$ (110) heterostructure, while reference [16] concerns only the electrical property of the heterostructure. Second, there is band-bending in the PDOS, and figure 5(c) of Ref. [16] shows that the top of the valence band moves toward Fermi level as it gets closer to the surface, in contrast, figure 5(b) of our work shows no such band-bending. This discrepancy comes from the different model structures. In our work, a symmetric model interface is employed without the vacuum layer. Owing to no intrinsic electrostatic field to avoid the polar catastrophe in our model structure, there is no such band-bending, which is in contrast to the results in the present work.[16] However, from Figs. 4 and 5, it can be seen that the two-fold degenerate d_{xz}/d_{yz} electrons contribute mainly to the 2DEG and magnetism of $LaAlO_3/SrTiO_3$ (110) heterostructure.

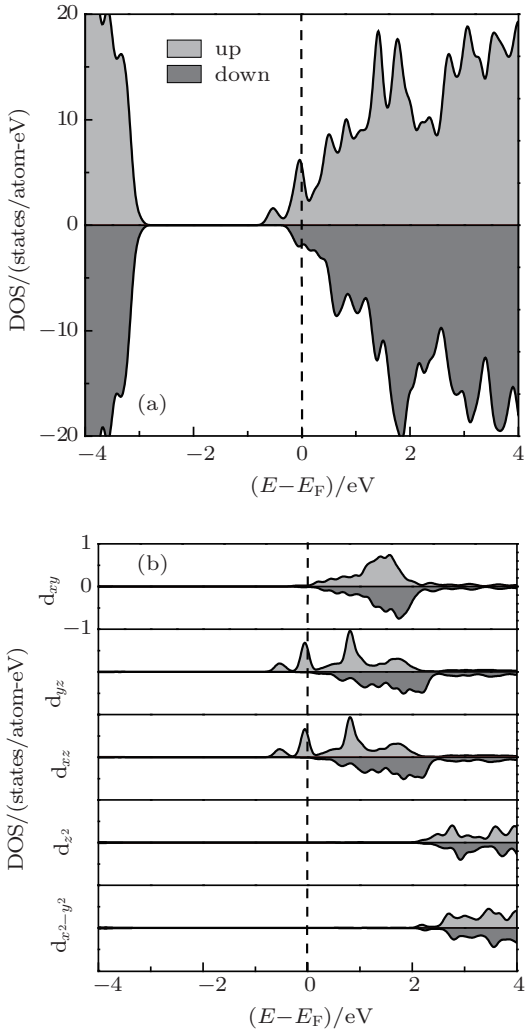


Fig. 4. (a) Total density of states (TDOS); (b) partial density of states (PDOS) of the Ti 3d states at the interface.

The band structure of the relaxed $LaAlO_3/SrTiO_3$ (110) heterostructure is shown in Fig. 6. The occupied conduction bands are characterized by a set of spin-polarized parabolic subbands. Combining with Fig. 4(b), we can see that these spin-polarized parabolic subbands correspond to the Ti 3d states. The three-fold degenerate t_{2g} orbitals split into the lower two-fold degenerate d_{xz}/d_{yz} and higher nondegenerate d_{xy} subbands. The more relevant feature is the large spin-splitting (~ 0.45 eV) of the lowest two-fold degenerate d_{xz}/d_{yz} subbands. The spin-splitting yields a magnetic moment of

about 0.35 μB on the Ti atom of the interface. Since the Ti–O octahedron distortions and the buckled interface structure give rise to a layer-dependent polarization, they may induce changes in the orbital structures and electron distributions of the heterostructure. To analyze this effect, we also calculate the band structure of ideal $LaAlO_3/SrTiO_3$ (110) interface. The results indicate that the magnetism of the 2DEG is negligible. This can demonstrate that the Ti–O octahedron distortions and the buckled interface structure play an important role in forming the magnetic 2DEG. In addition, the spin-splitting decreases with the decrease of the subband occupation as shown in Fig. 6. The higher occupied two-fold degenerate d_{xz}/d_{yz} subbands contribute to the magnetism mainly.

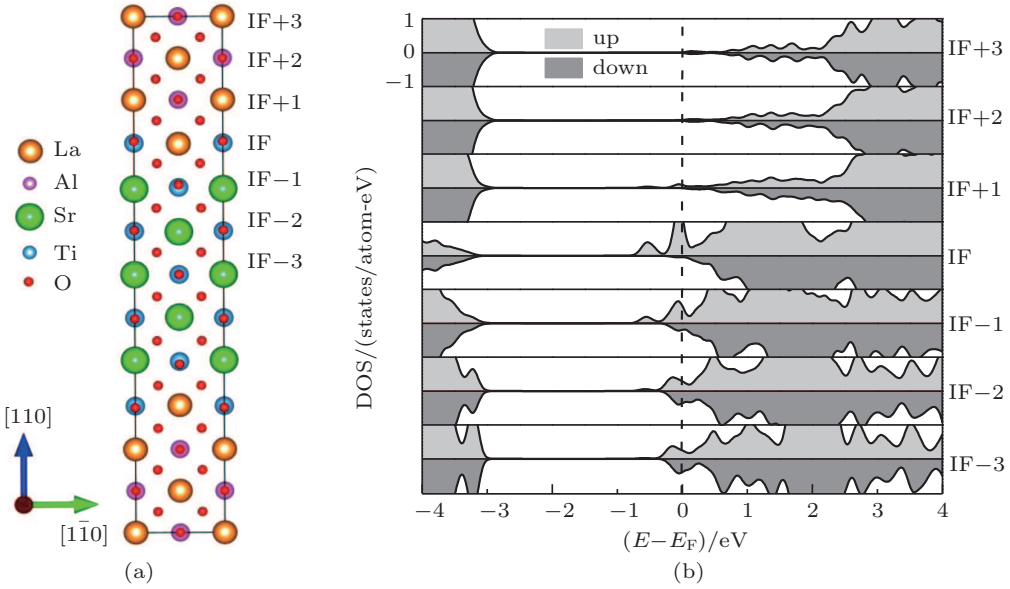


Fig. 5. (color online) (a) Relaxed $LaAlO_3/SrTiO_3$ (110) heterostructure with buckled interfaces; (b) the partial density of states grouped by layers of the heterostructure. The data (relaxed structure and PDOS) for each layer are aligned on the same vertical position. Here, the interface is denoted by IF.

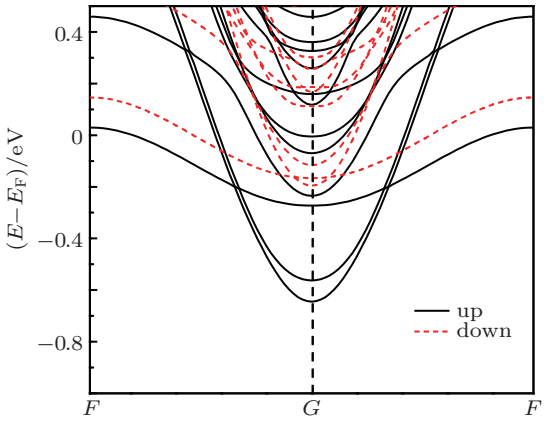


Fig. 6. (color online) Bands of the heterostructure of $LaAlO_3/SrTiO_3$ (110) as shown in Fig. 3.

4. Conclusion

From results of DFT calculations, we find that the buckled $LaAlO_3/SrTiO_3$ (110) interface is more stable than the abrupt $LaAlO_3/SrTiO_3$ (110) interface. Lattice mismatch between $LaAlO_3$ and $SrTiO_3$ leads to ferroelectric-like lattice distortions at the interface. The Ti–O octahedron distortions and the buckled interface structure are essential for the magnetic 2DEG. The partly filled two-fold degenerate d_{xz}/d_{yz} orbitals are the origin of 2DEG at the interface of $LaAlO_3/SrTiO_3$ (110). The spin-splitting of Ti 3d electrons is the origin of the magnetic property at the interface of $LaAlO_3/SrTiO_3$ (110).

References

[1] Ohtomo A and Hwang H Y 2004 *Nature* **427** 423
[2] Reyren N, Thiel S, Caviglia A D, Kourkoutis L F, Hammerl G, Richter C, Schneider C W, Kopp T, Retschi A S, Jaccard D, Gabay M, Muller D A, Triscone J M and Mannhart J 2007 *Science* **317** 1196
[3] Brinkman A, Huijben M, Van Zalk M, Huijben J, Zeitler U, Maan J C, Van der Wiel W G, Rijnders G, Blank D H A and Hilgenkamp H 2007 *Nat. Mater.* **6** 493
[4] Basletic M, Maurice J L, Carrétéro C, Herranz G, Copie O, Bibes M, Jacquet E, Bouzehouane K, Fusil S and Bar-thélémy A 2008 *Nat. Mater.* **7** 621
[5] Ariando, Wang X, Baskaran G, Liu Z Q, Huijben J, Yi J B, Annadi A, Barman A R, Rusydi A, Dhar S, Feng Y P, Ding J, Hilgenkamp H and Venkatesan T 2011 *Nat. Commun.* **2** 188
[6] Lee J S, Xie Y W, Sato H K, Bell C, Hikita Y, Hwang H Y and Kao C C 2013 *Nat. Mater.* **12** 703
[7] Dikin D A, Mehta M, Bark C W, Folkman C M, Eom C B and Chandrasekhar V 2011 *Phys. Rev. Lett.* **107** 056802
[8] Li L, Richter C, Mannhart J and Ashoori R C 2011 *Nat. Phys.* **7** 762
[9] Bert J A, Kalisky B, Bell C, Kim M, Hikita Y, Hwang H Y and Moler K A 2011 *Nat. Phys.* **7** 767
[10] Li J C, Beltrán J I and Muñoz M C 2013 *Phys. Rev. B* **87** 075411
[11] Wang H Y, Duan Z G, Liao W H and Zhou G H 2010 *Chin. Phys. B* **19** 037301

[12] Pentcheva R and Pickett W E 2009 *Phys. Rev. Lett.* **102** 107602
[13] Savoia A, Paparo D, Perna P, Ristic Z, Salluzzo M, Miletto Granozio F, Scotti di Uccio U, Richter C, Thiel S, Mannhart J and Marrucci L 2009 *Phys. Rev. B* **80** 075110
[14] Chen W H, Zhang R Z and Yang L N 2012 *Mater. Rev.* **26** 1 (in Chinese)
[15] Mukunoki Y, Nakagawa N, Susaki T and Hwang H Y 2005 *Appl. Phys. Lett.* **86** 171908
[16] Annadi A, Zhang Q, Wang X R, Tuzla N, Gopinadhan K, Lü W M, Roy Barman A, Liu Z Q, Srivastava A, Saha S, Zhao Y L, Zeng S W, Dhar S, Olsson E, Gu B, Yunoki S, Maekawa S, Hilgenkamp H, Venkatesan T and Ariando 2013 *Nat. Commun.* **4** 1838
[17] Herranz G, Sánchez F, Dix N, Scigaj M and Fontcuberta J 2012 *Sci. Rep.* **2** 758
[18] Bottin F, Finocchi F and Noguera C 2003 *Phys. Rev. B* **68** 035418
[19] Noguera C 2000 *J. Phys.: Condens. Matter* **12** R367
[20] Pojani A, Finocchi F and Noguera C 1999 *Surf. Sci.* **442** 179
[21] Eglitis R I and Rohlfing M 2012 *Phys. Status Solidi B* pp. 1–7 (Wiley Online Library)
[22] Blöchl P E 1994 *Phys. Rev. B* **50** 17953
[23] Kresse G and Furthmüller J 1996 *Phys. Rev. B* **54** 11169
[24] Kresse G and Joubert D 1999 *Phys. Rev. B* **59** 1758
[25] Liechtenstein A I, Anisimov V I and Zaanen J 1995 *Phys. Rev. B* **52** R5467
[26] Mizokawa T and Fujimori A 1995 *Phys. Rev. B* **51** 12880
[27] Monkhorst H J and Pack J D 1976 *Phys. Rev. B* **13** 5188
[28] Chakhalian J, Millis A J and Rondinelli J 2012 *Nat. Mater.* **11** 92